Catalysis Science & Technology

Accepted Manuscript

This article can be cited before page numbers have been issued, to do this please use: L. Wang, Y. Zhang, X. Gu, Y. Zhang and H. Su, *Catal. Sci. Technol.*, 2017, DOI: 10.1039/C7CY02304A.

ROYAL SOCIETY OF CHEMISTRY

rsc.li/catalysis

View Article Online
DOI: 10.1039/C7CY02304A

Journal Name

ARTICLE

Insight into the Role of UV-Irradiation in Photothermal Catalytic Fischer-Tropsch Synthesis over TiO_2 Nanotube Supported Cobalt Nanoparticles

Received 00th January 20xx,
Accepted 00th January 20xx

DOI: 10.1039/x0xx00000x

www.rsc.org/

Limin Wang, Yichi Zhang, Xiaojun Gu,* Yulong Zhang and Haiquan Su*

To explore an efficient catalytic system with high activity and selectivity is the key to improve Fischer-Tropsch synthesis (FTS) technology and the main focus in academic field. Herein, a photothermocatalytic system for FTS was constituted by combining thermo-active component with photo-sensitive support. The 20 wt% and 30 wt% Co supported TiO_2 nanotube (TNT) catalysts were prepared through incipient wetness impregnation method (named as 20% Co/TNT and 30% Co/TNT), and were applied to photothermocatalytic process to investigate the role of ultraviolet (UV) illumination in the traditional thermochemical FTS reaction. The results indicated that introduction of UV light dramatically improved CO conversion, from 9.2% to 64.0% for 20% Co/TNT and from 8.6% to 17.1% for 30% Co/TNT. In addition, UV illumination gave rise to an increase in light paraffin selectivity. The improvement of CO conversion was found to be related to the photogenerated electrons transfer from TNT to active Co sites upon UV light irradiation, and this caused the Co sites with increased surface electron density and subsequently enhanced the adsorption and activation of CO molecules at Co sites. While the increase in light paraffin selectivity was attributed to the photo-promoted hydrogenation of olefin and the hydrogenolysis of the long-chain hydrocarbons. The present work promoted a deeper understanding of the photothermal FTS reaction mechanism and demonstrated that photothermocatalysis could be a potential for enhancing FTS catalytic performance and adjusting product distribution.

1. Introduction

Fischer-Tropsch synthesis (FTS) is an effective heterogeneous catalytic route to convert syngas (mixture of CO and H_2) into various hydrocarbons, including gasoline, diesel oil and other chemicals, which has received wide-spread attention nowadays due to both the dwindling nonrenewable energy sources and the diversified source of syngas (e.g. natural gas, coal and biomass).[1–3] Low catalytic productivity and the broad product distribution of FTS place severe limitations on its attractiveness as a commercial operation. Hence, higher CO conversion and desired selectivity are critical design criteria in FTS. To address above issues, for decades tremendous traditional endeavors have been devoted to the development of FT technology, such as optimizing catalyst structure (active metal particle size, support, promoter, etc.), tuning the reaction parameters (temperature, pressure, space velocity, etc.) and even designing various reactor type (fixed bed, slurry bed, stirred basket, etc.),[4–6] and significant progresses have been achieved. Nonetheless, all of the above attempts are limited on the thermocatalytic domain, which is an energy-consuming process by using an additional heater.

Compared with thermochemical reaction, photocatalysis is one of the most sustainable, reliable, and economical and eco-friendly solutions to solve energy and environmental issues by using solar energy as the driving force.[7] It has been extensively studied as a promising technology for hydrogenation reaction, including carbon dioxide hydrogenation,[8,9] selective hydrogenation of nitroaromatics,[10, 11] and hydrogenation of carbonyl compounds,[12,13] etc. For example, Pd/TiO_2 has been reported to show superior activity for the photocatalytic hydrogenation of CO_2 under UV illumination.[14] The architecture of $CdS/H_2Ti_5O_{11}$ ultrathin nanobelt displayed almost 100% yield with a selectivity of about 98% in 3 min under visible light irradiation for converting 4-nitroaniline to *p*-phenylenediamine.[15] In 2011, Mul et al. have made an attempt to photocatalytically hydrogenate CO by exposing Ti-SBA-15 to 120 W high-pressure mercury lamp irradiation.[16] The result showed that just trace amount of CH_4, C_2H_4 and C_2H_6 were produced, inferring that CO molecule cannot be effectively activated by sole illumination possibly maybe owing to the limited light energy utilization in photocatalytic technique. On the basis of above results, we thought that if a photothermal catalytic system with which thermal energy can be coupled with photonic energy could be established to drive FTS process,

Inner Mongolia Key Laboratory of Coal Chemistry, School of Chemistry and Chemical Engineering, Inner Mongolia University, Hohhot 010021, China. E-mail: xiaojun.gu@yahoo.com, haiquansu@yahoo.com; Fax: +86-471-499-2981; Tel: +86-471-499-2981

† Electronic Supplementary Information (ESI) available: PXRD, XPS, TEM, Raman, N_2 adsorption-desorption isotherms, UV-vis absorption spectra of used 20% Co/TNT catalyst, and the experimental results for Fischer-Tropsch synthesis over TNT support. See DOI: 10.1039/x0xx00000x

View Article Online
DOI: 10.1039/C7CY02304A

it might lead to distinct new possibilities towards the production of renewable fuels. Our initial study and other two group's results demonstrated the general applicability of the photothermocatalytic process for the synthesis of hydrocarbon compounds.[17–19] However, the insight into the mechanism, such as the possible reaction pathways, the role of electrons and holes, actual rate-determining elementary step, as well as underlying synergism effects between light and thermal effects has not been explored and needs to be deeply extensively studied.

In this context, the development of efficient catalytic active component and suitable photosensitizer is of prime importance. Supported Co-based catalysts show the good thermo-catalytic activity for CO hydrogenation reaction and are more advantageous in the commercial FTS process.[20,21] Titanium dioxide (TiO_2), a totally environmentally benign photo-sensitive semiconductor, has been regarded as the common support in FTS reaction over the past decades due to its strong metal-support interaction (SMSI) and better stability.[22–24] Compared with nanoparticles, TiO_2 in the form of nanotubes should be a preferred support material for the harsh FTS reaction condition due to its high surface area for active site exposure, unique electronic characteristics, a superior physical topology, as well as good heat transfer properties.[25–27]

Based on the above considerations, in this work we intentionally combined photo-sensitive TiO_2 nanotube (TNT) with thermo-active Co to constitute a bifunctional Co/TNT catalyst. TNT as a photo-sensitive species was motivated under UV illumination to generate the reactive electrons and holes, while cobalt as a thermocatalyst loaded on the surface of TNT could weaken C-O bonds and couple C-C bonds. Considering the adsorption and activation of CO are favored over the metal nanoparticles with higher electron density,[28–30] it can be envisioned that under UV light irradiation the photogenerated electrons of TiO_2 would be transferred to active Co sites due to the difference in work function between metal and semiconductor, leading to the electron density enrichment of active Co sites and the resulting superior catalytic performance on CO hydrogenation under photothermocatalytic condition. Thus a photothermocatalytic process for driving FTS reaction over TNT supported cobalt catalysts with different loadings was explored, and the influence of UV illumination on the activity and the product distribution during the FTS reaction were investigated by some control experiments, in-situ Raman and other characterizations. A possible reaction mechanism was tentatively proposed.

2. Experimental

2.1 Catalyst preparation

TNT was prepared by a hydrothermal method according to previous reports.[31] Typically, 1.25 g of anatase TiO_2 powder was dispersed into NaOH solution (8 M, 125 mL). The suspension was transferred into a Teflon-lined container (200 mL) sealed in a stainless steel autoclave and was kept at 423 K for 48 h. The obtained white precipitate was washed with hydrochloric acid (pH = 1.0) until the pH value of the suspension turned into 7.0. After filtration, the powder was washed with H_2O and ethanol for several times and then dried at 353 K. Finally, the powder was calcined at 673 K for 12 h to obtain the TNT.

The TNT supported catalysts containing 20 wt% and 30 wt% cobalt were prepared by the incipient wetness impregnation method. TNT was impregnated by an aqueous solution of $Co(NO_3)_2{\cdot}6H_2O$. After impregnation, the sample was dried at 353 K overnight and then calcined in an air flow at 673 K for 3h. The pure Co_3O_4 sample used in Raman test was obtained by calcining $Co(NO_3)_2{\cdot}6H_2O$ powder in an air flow at 673 K for 3 h.

2.2 Characterizations

The powder X-ray diffraction (PXRD) characterization was performed on a Panalytical X'pert Pro diffractometer with Cu Kα radiation (40 KV, 40 mA). The scan speed was 25.068 °/min, with a scanning angel ranged from 5° to 90°. H_2-TPR measurements of the prepared catalysts were carried out using a AutoChem II 2920 equipped with a TCD detector. Ultraviolet-visible spectra were collected in the range of 200-800 nm using a UV-3600 Shimadzu spectrometer. The textural properties of the support and the corresponding catalysts were determined by the N_2 adsorption-desorption test performed on a Micrometrics ASAP2020 analyzer. The structures of samples were characterized with a FEI Tecnai G2 F20 S-Twin transmission electron microscope at 200 KV. Raman spectra were recorded on a LabRAM HR Evolution Raman spectrometer with an excitation of 514 nm laser light. X-ray photoelectron spectra were collected on a Thermo Fisher Scientific ESCALAB 250Xi photo electron spectrometer. CO-TPD measurements of the samples were conducted using the same apparatus that was used for TPR to analyze the CO adsorption ability on the used catalysts after Fischer-Tropsch synthesis reaction for approximately 55 h under UV irradiation and in the dark. For TPD testing, 90 mg of the used catalyst was packed in a quartz U-tube, flushed with Ar for 30 min at 373 K and then cooled down to 323 K slowly. Subsequently, the samples were exposed in CO gas flow at 323 K for 60 min, and then Ar was introduced to allow physisorbed CO to desorb and to clear the apparatus of gas phase CO. After there was no CO signal detected in the trail gas, the sample was heated from 323 K to 1173 K at a rate of 10 K/min while the thermal conductivity of the sample tube effluent was monitored. H_2-O_2 titrations were also carried out in 2920 II Micromeritics system with a thermal conductivity detector to measure the dispersion of cobalt in Co/TNT catalysts. Before the measurements, the samples were completely reduced by 10 vol.% H_2/Ar at 885 K and subsequently preoxidized in O_2 at 373 K and outgassed in an Ar flow at 373 K for 2 h; then, pulses of H_2 were sent to the sample until complete saturation was reached. Operando Raman spectra were obtained in an in situ reaction cell unit to test the chemisorption of CO on sample under different excitation. Before measurements, the 20% Co/TNT catalyst were completely reduced in situ at 885 K under atmospheric pressure with a stream of hydrogen. The

View Article Online
DOI: 10.1039/C7CY02304A
Journal Name ARTICLE

temperature was then cooled to 298 K, after which the catalyst was then exposed to high purity CO (>99.99%) for 60 min. Raman spectra were recorded with a 633 nm light laser in the range between 1750 and 2200 cm^{-1}. For testing CO chemisorption under UV light irradiation, a 325 nm light laser was selected to excite Raman spectra.

2.3 Catalytic activity test

Hydrogenation of CO was conducted with a self-designed apparatus consisting of a stainless reaction chamber with a quartz window in the middle for light irradiation (As shown in Fig. SI) . The volume of the chamber was 2.4 L, in which the catalyst bed could be both heated and irradiated. Catalyst sample (1.2 g) was dispersed in 10.0 mL ethanol with the aid of an ultrasonic bath. Subsequently, the obtained suspension was coated on ten pieces of quartz (290 mm×65 mm×1.6 mm), then the quartz was perpendicularly inserted in the edge of stainless steel reactor. In order to inspect the influence of the illumination on catalytic activity and selectivity, all the samples (including TNT support and Co/TNT catalysts) were tested under three different conditions: photocatalytic process (with only UV irradiation), thermocatalytic process (with heat under dark), and photothermocatalytic process (with both heat and UV irradiation), respectively. Prior to the reaction, the chamber was evacuated by a mechanical pump. Then, the catalyst was reduced for 10 h at 360 °C under pure hydrogen flowing at 28 ml/min at atmospheric pressure. After the treatment, the reactor was cooled down to 50 °C. Then the syngas($CO/H_2/Ar$=20:10:1 WSHV=1400 mL/h·g) was introduced into the reactor and the pressure was increased to 2.0 MPa. After that, the catalyst was slowly heated to 220 °C. During the photothermocatalytic process, the sample was irradiated by UV light (produced by a 500 W Hg lamp) from the top of the reactor via a cylindrical quartz window. Meanwhile, integration of circulating thermostated water through an outer jacket around the lamp was carried out to prevent the heat generated by the lamp from reaching the reactor. The reaction products were continuously removed from the reactor. The heavy hydrocarbons and most of the water were condensed in two traps kept at 120 °C and 0.5 °C, respectively, and the tail gas (C_1–C_4 hydrocarbons, CO_2, Ar and unconverted CO) was analyzed online by gas chromatograph (GC-2014C, Shimadzu) equipped with two detectors (a TCD and a FID). Ar in the feed gas was used as internal standard to calculate CO conversion, and the CO conversion and product selectivity parameters are defined as:

$$\text{CO conversion}\ (\%)=\frac{(A_{CO}/A_{Ar})_{in}-(A_{CO}/A_{Ar})_{out}}{(A_{CO}/A_{Ar})_{in}}\times 100$$

$$S_{CO_2}(\%)=\frac{n_{CO_{2,out}}}{n_{CO_{in}}\times \text{CO conversion}}\times 100$$

$$S_{C_i}(\%)=\frac{n_{product\ out}\times \text{carbon number}}{n_{CO_{in}}\times \text{CO conversion}-n_{CO_{2,out}}}\times 100\ \ (i=1, 2, 3, 4)$$

$$S_{C_{5+}}(\%)=100-\sum_{i=1}^{4} S_{C_i}(\%)$$

Where A represents corresponding peak area and n is the number of moles.

3. Results and discussion

3.1 Characterization of catalysts

The crystallographic structure and phases of the synthesized TNT and fresh Co/TNT catalysts were determined by PXRD as illustrated in Fig. 1. Diffraction lines assigned to anatase TiO_2 (PDF#:21-1272) and Co_3O_4 (PDF#:42-1467) were observed from the PXRD patterns. Peaks of other cobalt compounds such as CoO and Co-titanate were not detected. Co_3O_4 has a spinel-type structure, in which oxygen atoms are arranged in fcc and Co^{2+} and Co^{3+} cations are located in tetrahedral and octahedral coordination, respectively.[32] Moreover, it was found that the diffraction intensities of anatase TiO_2 dramatically decreased due to the decrease of TiO_2 ratio when increasing cobalt loading from 20 wt% to 30 wt%. The crystallite sizes of Co_3O_4 estimated from the most intense diffraction line at 2θ = 36.8° using the Scherrer equation were shown in Table 1. Table 1 also summarized the metal dispersion evaluated from H_2-O_2 titration. As shown, a better dispersion was obtained in 20% Co/TNT compared with that in 30% Co/TNT, which was in agreement with the crystallite diameter obtained from XRD estimation.

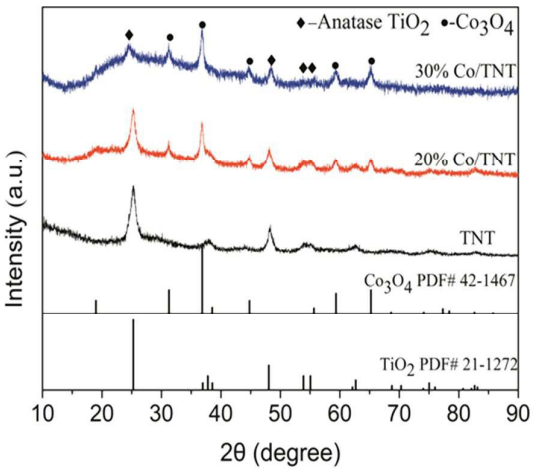

Fig. 1 PXRD patterns of TNT support and fresh Co/TNT catalysts.

Representative TEM images of the TNT support and the Co/TNT catalysts were shown in Fig. 2. The results showed that the TiO_2 support had mainly one-dimensional nanotubular morphology with open ends, featuring 200–400 nm of length and ca.5–6 and 8–10 nm of inner and outer diameter, respectively. From Fig. 2d and 2g, it could be clearly seen that the Co_3O_4 nanoparticles were dispersed on the surface of TNT.

View Article Online
DOI: 10.1039/C7CY02304A

Table 1 Physicochemical properties of as-prepared TNT and Co/TNT catalysts.

Sample	d_{Co3O4} (nm)	Dispersion (%)	BET area (m^2/g)	Pore diameter (nm)	Total pore volume (cm^3/g)
TNT	–	–	182	17.5	1.01
20% Co/TNT	12.6	2.18	138	3.4	0.82
30% Co/TNT	16.3	1.76	133	3.4	0.30

Dispersion (%): cobalt metal dispersion obtained from H_2-O_2 titration

The sizes of Co_3O_4 nanoparticles were in the range of 8 nm–12 nm for 20% Co/TNT and 11–16 nm for 30% Co/TNT, which were roughly in agreement with the crystallite sizes estimated from XRD patterns. From the TEM and the data in Table 1, it could be concluded that the extent of cobalt oxide aggregation for the 30% Co/TNT catalyst was more serious than that for the 20% Co/TNT. Meanwhile, Fig. 2e and Fig. 2h displayed the HRTEM images of 20% Co/TNT and 30% Co/TNT respectively. The clear fringe spacing values of 2.86 Å and 2.06 Å were corresponding to (220) and (400) planes of Co_3O_4, respectively, which was in accordance with XRD phase identification. The corresponding energy-dispersive X-ray spectroscopy (EDS) for each sample was also tested, clearly showing the expected metal element signals (Fig. 2c, 2f, and 2i).

The BET surface area, total pore volume, and average pore diameter of the TNT support and freshly prepared Co/TNT catalysts had been characterized. The results were presented in Table 1. Surface area and pore volume significantly decreased after cobalt loaded on TiO_2, suggesting that the cobalt oxide particles were deposited into the pores or blocked the pore channels of the TNT support.[33] Adding 20 wt% and 30 wt% of cobalt decreased the BET surface area from 182 to 138 m^2/g and 182 to 133 m^2/g, respectively. In addition, the pore volume decreased from 1.01 to 0.82 cm^3/g for 20 wt% Co and from 1.01 to 0.30 cm^3/g for 30 wt% Co. These values indicated that pore blockage for 30% Co/TNT was higher than that for 20% Co/TNT.

Optical properties are primarily important in connection with the photocatalytic activity. Fig. 3 showed UV-visible absorption spectra of the samples. Pristine TNT had UV-absorption band in the range of 200-385 nm. The Co_3O_4 loaded surface caused strong absorption in the visible region. Broad absorption ranging from 400–750 nm was attributed to the d–d transitions of Co^{2+} and Co^{3+} ions located in the tetrahedral and octahedral coordination spheres.[34]

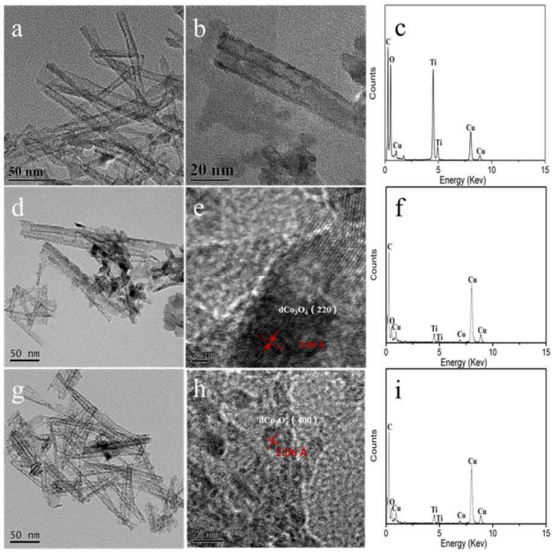

Fig. 2 TEM images and the corresponding EDS patterns of TNT and fresh Co/TNT catalysts: (a, b, c) TNT; (d, e, f) 20% Co/TNT; (g, h, i) 30% Co/TNT.

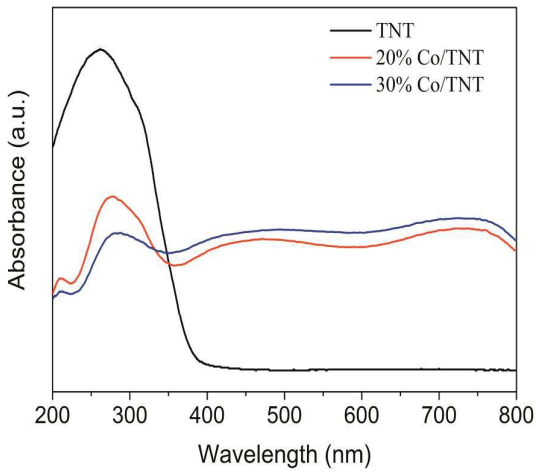

Fig. 3 UV-vis absorption spectra of TNT support and fresh Co/TNT catalysts.

View Article Online
DOI: 10.1039/C7CY02304A

The reduction behaviour of the Co/TNT catalysts was studied by H_2-TPR, as displayed in Fig. 4. The TPR profiles of the catalysts were characterized by three main reduction stages the first peak (192 °C–347 °C) was associated with the reduction of Co_3O_4 to CoO, while the second one (347 °C–612 °C) corresponded to the reduction of CoO to metallic cobalt,[35, 36] and the third peak (> 790 °C) was the reduction of cobalt species with strong Co-TiO_2 interaction, as previously reported in literatures.[37] It should be noted that the area under the TPR peaks was proportional to the amount of H_2 consumed by cobalt oxide during the reduction process. The area under the TPR peaks for 30% Co/TNT was approximately 0.5 times larger than that for 20% Co/TNT catalyst.

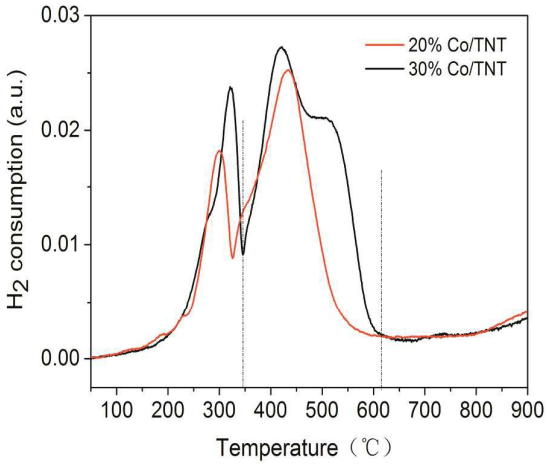

Fig. 4 H_2 consumption profiles during temperature programmed reduction for the freshly synthesized Co/TNT catalysts

The surface chemical composition and electronic state of Ti and Co for TNT support and as-prepared Co/TNT catalysts were determined by XPS. In the Ti 2p XPS spectra (Fig. 5a), two strong peaks of Ti $2p_{3/2}$ and Ti $2p_{1/2}$ centered at approximately 458.6 and 464.4 eV, respectively. The shapes and energy positions were nearly the same for the catalysts and pure TNT sample, which agreed well with the TiO_2 values reported.[38] Co 2p XPS spectra were shown in Fig. 5b. Two main peaks containing $2p_{3/2}$ state and $2p_{1/2}$ state with two shake-up satellite peaks were observed from the Co photoelectron spectra of catalysts, and the binding energy between the Co $2p_{1/2}$ and Co $2p_{3/2}$ peak was about 15.6 eV, corresponding to the characteristic peaks of the standard Co_3O_4.[39,40] Furthermore, the results exhibited that binding energies of Co $2p_{3/2}$ and Co $2p_{1/2}$ in 20% Co/TNT slightly shifted to lower values compared to those in 30% Co/TNT, indicating that the electronic density of Co ions in the 20% Co /TNT catalyst was higher than that in 30% Co/TNT catalyst. This might be due to strong interaction between cobalt oxide and support.[41]

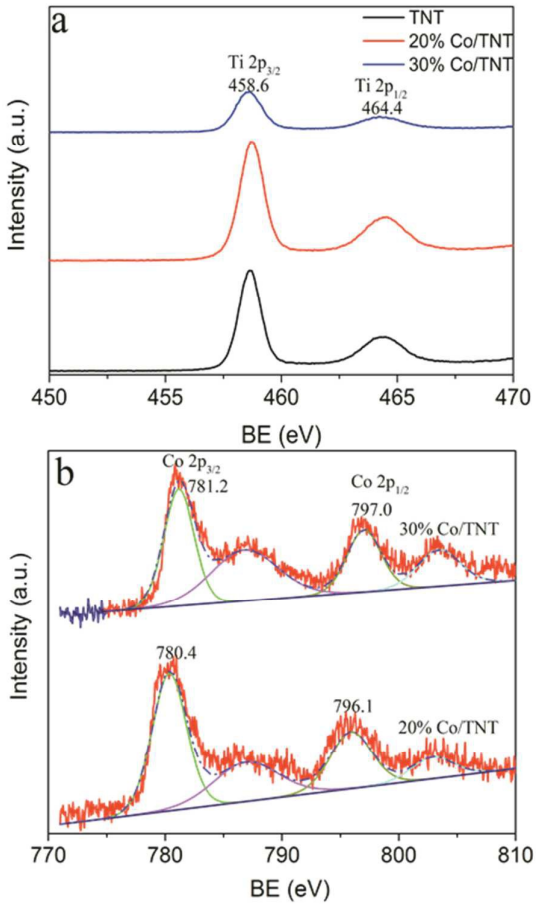

Fig. 5 XPS spectra of fresh Co/TNT samples with different Co loadings: (a) Ti 2p and (b) Co 2p.

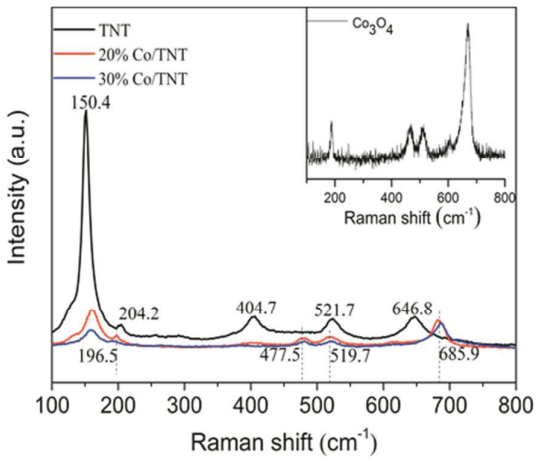

Fig. 6 Raman spectra of TNT support and fresh Co/TNT catalysts, and pure Co_3O_4 sample (inset).

View Article Online
DOI: 10.1039/C7CY02304A

Fig. 6 showed the laser Raman spectra of the TNT support, fresh Co/TNT catalysts and pure Co_3O_4 samples. The results showed that the vibration bands of anatase TiO_2 were located at 150.4 cm^{-1} (E_g), 204.2 cm^{-1} (E_g), 404.7 cm^{-1} (B_{1g}), 521.7 cm^{-1} (A_{1g}), and 646.8 cm^{-1} (E_g).[42, 43] After Co_3O_4 loading, the Raman vibration peaks of anatase TiO_2 were blue-shifted, and such shift could be attributed to an interaction between TiO_2 and cobalt species and disorder in the oxygen sublattice.[44] New vibration bands appeared at 196.5 cm^{-1}, 477.5 cm^{-1}, 519.7 cm^{-1} and 685.9 cm^{-1} could be assigned to F_{2g}, E_g, F_{2g}, and A_{1g} of Co_3O_4, respectively,[45,46] which was in accordance with the spectrum of pure Co_3O_4 sample (inset in Fig. 6).

3.2 Catalytic performance and mechanism

The CO hydrogenation performance was examined under the pressure of 2.0 MPa for 55 h. The results of photocatalysis, thermocatalysis and photothermocatalysis of TNT support and Co/TNT with two different Co loadings for FTS at the steady-state regime after 40 h on stream were shown in Table 2 and Table S2. Some control experiments were also carried out. It was easy to see that the sole UV irradiation was unable to catalyze CO hydrogenation for TNT or Co/TNT catalyst, revealing that the temperature was required to obtain kinetics for overcoming activation barrier. Even if the temperature reached 220 ^oC, compared with that over the cobalt loaded catalysts, the CO conversion over the TNT was very low and less than 2% whether under UV illumination or not (as shown in Table S2), indicating that Fischer-Tropsch active metal component (Co in this work) indeed played an indispensable role in activating and subsequently dissociating CO, and further initiating carbon chain growth. Moreover, it was noteworthy that the photocatalysis significantly affected the activity and product selectivity. The CO conversion as function of time on stream under UV light irradiation and in the dark was presented in Fig. 7 for the cobalt loaded catalysts. The catalytic activity became stable after 25 h. With the introduction of the UV light, the conversions of CO increased over all Co/TNT catalysts. For 20% Co/TNT catalyst, the CO conversion was 9.2% in dark reaction, which was lower than that of other Co-based catalysts reported in literatures. Its low activity was attributed to only partial reduction from cobalt oxide to Co^0 after in situ pretreatment at 360 ^oC under H_2 flow, slight aggregation of metal nanoparticles because of high loading, and intrinsic feature of anatase TNT support.[47, 48] While it surprisingly increased to 63.9% with UV irradiation under the same temperature and pressure. Therefore, the light-enhanced activity is 54.7%. This result indicated that the UV irradiation could drastically enhance the intrinsic catalytic ability of Co/TNT for FTS. The enhanced activity was mainly attributed to the presence of illumination which facilitated CO dissociation. In the thermocatalytic process, TiO_2 just played a role of support to disperse and stabilize the active metal species; while in the photothermocatalytic process, TiO_2 was not only a support but also an efficient photococatalyst. Upon UV excitation of TiO_2, the electrons in VB will be excited to CB, leaving holes in VB. Because the work function of a metal is usually larger than that of semiconductor TiO_2,[49] the most commonly invoked mechanism for metal cocatalysts on photoactive TiO_2 is that the metal sites behave as electron acceptors, resulting in an increase in the electron density on cobalt surface sites. The holes migrate to the TiO_2 surface and probably could be trapped by the reduced species in system, including water,[50, 51] hydrocarbon products,[52] CO or H_2,[53] while the concrete route is very complex and not clear, because some products or intermediates are unstable or difficult to detect and quantify. When CO molecules were adsorbed on Co active sites, the back donation of electrons from Co d orbital to the π* orbital of CO molecules could weaken the C–O strength and thus activated and dissociated CO molecules, which was a critical step reported in the literature that largely determined the activity of FTS reaction.[17,54,55]

Table 2 Performance of x% Co/TNT (x = 20, 30) for FTS under photothermocatalytic condition and thermocatalytic condition.

Catalyst	Condition	CO Conversion (%)	CO_2 Selectivity (%)	Hydrocarbon Selectivity (%)			Distribution in C_2-C_4 (%)	
				CH_4	C_2-C_4	C_{5+}	Paraffin	Olefin
20% Co/TNT	30 ^oC +UV light	–	–	–	–	–	–	–
	220 ^oC	9.2	21.6	24.7	33.6	41.7	89.0	11.0
	220 ^oC+UV light	63.9	17.3	34.6	22.7	42.7	98.6	1.4
30% Co/TNT	30 ^oC +UV light	–	–	–	–	–	–	–
	220 ^oC	8.6	17.9	23.1	36.2	40.7	83.0	17.0
	220 ^oC+UV light	17.1	8.4	31.5	32.5	36.0	97.7	2.3

Reaction conditions: CO/H_2 = 1/2, flow rate = 28 ml min^{-1}, pressure of 2.0 MPa, temperature of 493 K, catalyst (1.2 g). The hydrocarbon selectivities were normalized with the exception of CO_2.

View Article Online
DOI: 10.1039/C7CY02304A

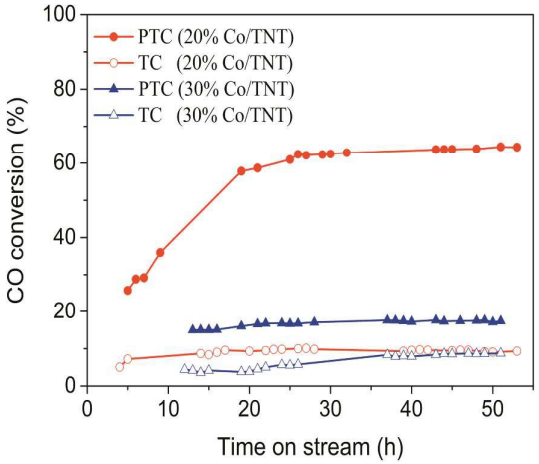

Fig. 7 Plots of CO conversion against time on stream under two catalytic conditions for 20% Co/TNT and 30% Co/TNT (where TC and PTC represent thermocatalysis and photothermocatalysis, respectively).

In order to verify the weakening effect of Co on C–O bond in CO molecules, we further investigated the CO adsorption behavior over 20% Co/TNT under UV irradiation (325 nm laser excitation) and visible irradiation (633 nm laser excitation) by in situ Raman, respectively. As seen in Fig. 8, the peaks at 2140 cm^{-1} could be attributed to gaseous carbon monoxide and the peaks at about 1917 cm^{-1} was due to the bridged CO adsorbed on cobalt metals. [56, 57] When excited with 633 nm laser for which TNT fairly had no absorption, the 20% Co/TNT only exhibited an apparent peak at 2140 cm^{-1}, indicating the bridged-type adsorbed CO was negligible, which would result in lower CO conversion under thermocatalytic condition as listed in Table 2. While with the introduction of 325 nm UV laser excitation for which TNT had a very strong absorption, a low-frequency peak at about 1917 cm^{-1} assigned to bridged CO adsorbed on cobalt metal was also observed besides gaseous CO.[58] According to Weaver and coworkers, adsorption at bridge bonded sites generally need a long exposure time even from nearly saturated CO solutions.[59] This indicated that the introduction of UV light does promote the adsorption of CO at Co sites. As reported by many researchers, the bridge-type CO is much more active for the FT reaction due to a weaker C–O bond that can be more easily dissociated to carbon and oxygen atoms,[60,61] thus, high CO conversion was obtained under UV illumination in this work. Concerning that UV illumination is more likely to change the catalyst structure and hence resulted in different activities and selectivities, the physical, chemical and photoelectric properties of spent 20% Co/TNT composite after the test of photothermocatalytic and thermocatalytic FTS were thoroughly characterized by PXRD (Fig. S2), XPS (Fig. S3), TEM (Fig. S4), Raman spectra (Fig. S5), BET technique (Fig. S6 and Table S1), and UV-vis absorption spectra (Fig. S7). No obvious difference was found between two conditions in such kinds of characterization results, thus the much higher photothermocatalytic activity compared to the thermocatalytic activity originated from other factors rather than catalyst structure. This photo-assisted CO conversion phenomenon was also observed over 30% Co/TNT. The CO coneversion of 17.9% and 8.4% were obtained under UV light irradiation and in the dark, respectively. The light-enhanced activity was 9.5%, which was smaller than that over 20% Co/TNT. Such results might be caused by the different amounts of photogenerated electrons transferred from TiO_2 to active metal nanoparticles, which could result in the adsorption and activation of different amounts of CO molecules.

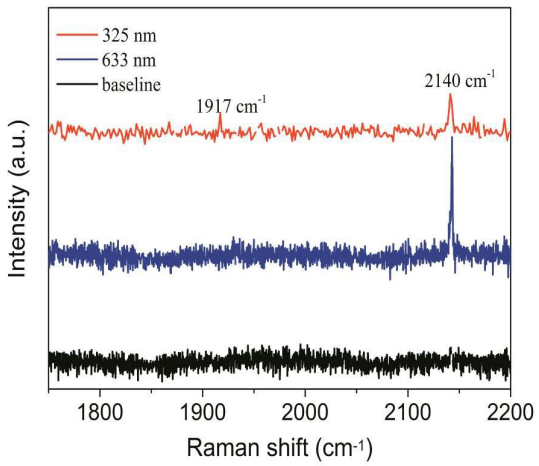

Fig. 8 In situ Raman spectra of adsorbing CO over H_2-reduced 20% Co/TNT under different laser excitation conditions.

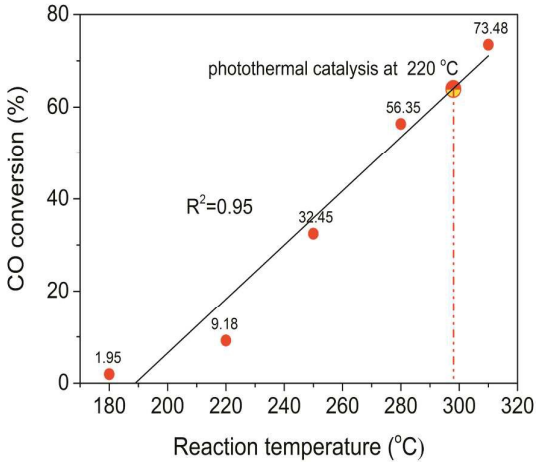

Fig. 9 CO conversion as a function of temperature for non-illuminated 20% Co/TNT catalysts.

Additionally, we demonstrated the thermocatalytic FTS at different temperatures for 20% Co/TNT catalyst. Fig. 9 revealed a linear increase of the CO conversion upon elevating the temperature. It was observed that the CO conversion at 220 °C/UV irradiation was comparable to that at 298 °C in dark condition. In other words, for achieving the same CO conversion, light-assisted thermocatalysis could be operated at

View Article Online
DOI: 10.1039/C7CY02304A

lower temperatures than their conventional counterparts that use only thermal stimulus. Thus, photothermocatalysis process is an energy-saving process compared to thermocatalytic process.

With respect to the product selectivity, as displayed in Table 2, the CO_2 selectivity under irradiation was lower than that without irradiation for all the catalysts, suggesting that water gas shift (WGS) reaction was restrained in photothermal condition. The decrease of the WGS reaction activity was most probably due to the decrease in water partial pressure caused by the oxidation of water by the photogenerated holes.[62] As for the product distribution within the hydrocarbon fraction, the high selectivity to short chain paraffins in thermocatalytic process was dependent on the the character of apparatus. The big volume (2.4 L) increases the residence time of formed FT products, probably resulting in that olefins were readsorbed on the active sites and initiate secondary reactions to produce CH_4 and C_2-C_4 paraffins. The CH_4 selectivity increased from 24.7% to 34.6% for 20% Co/TNT and from 23.1% to 31.5% for 30% Co/TNT at the expense of C_2-C_4 formation or C_{5+} formation under illumination, which might be caused by the photohydrogenolysis of long-chain hydrocarbons or direct hydrogenation of surface CH_x intermediates into lower hydrocarbons under UV irradiation. Such hydrocarbons hydrogenolysis reaction under light irradiation has been previously documented using TiO_2 [63, 64]and Ni-525[18] as catalyst, respectively. In addition, another pathway that favoring CH_x intermediates hydrogenated to CH_4 instead of chain growth is also possible due to excess H_2 dissociated on the catalyst surface under UV irradiation. Besides, the effect of illumination on paraffin/olefin distribution in the range of C_2-C_4 was presented in Fig. 10. It was notable that for 20% Co/TNT the alkanes represented 98.6% of the whole C_2-C_4 hydrocarbons under illumination, which was 9.6% higher than its corresponding value in the dark. Correspondingly, olefin decreased by 9.6% from 11.0% to 1.4%. Similar variation tendency was observed for 30% Co/TNT catalyst. To further investigate the origin of the observed change of paraffin/olefin distribution in the range of C_2-C_4 during illumination, additional experiments were conducted as follows: a standard gas mixture (H_2: 85%, C_2H_4: 5%, C_3H_6: 5%, C_4H_8: 5%) was introduced to reactor as initial reactants to achieve a pressure of 2.0 MPa, then the reaction system was kept in the absence of catalyst for 20 h under three different specified reaction conditions (25 °C with UV light radiation, 220 °C without light irradiation and 220 °C with UV light irradiation). The reactants and products were quantified online by the FID detector of Shimadzu GC-2014. The experimental results were shown in Fig. 11 and Table 3. It was obvious that no concentration changes could be observed for various components at 25 °C with UV light radiation. When heating the system to 220 °C, the concentration of all alkenes (C_2H_4, C_3H_6, C_4H_8) decreased, and correspondingly, some alkanes (C_2H_6, C_3H_8 and C_4H_{10}) appeared, indicating alkenes were converted into alkanes by hydrogenation. However, the reactor we used is made of 0Cr18Ni9 stainless steel which contains 18.00～20.00% Cr and 8.00～10.50% Ni, and it is most possible that these transition

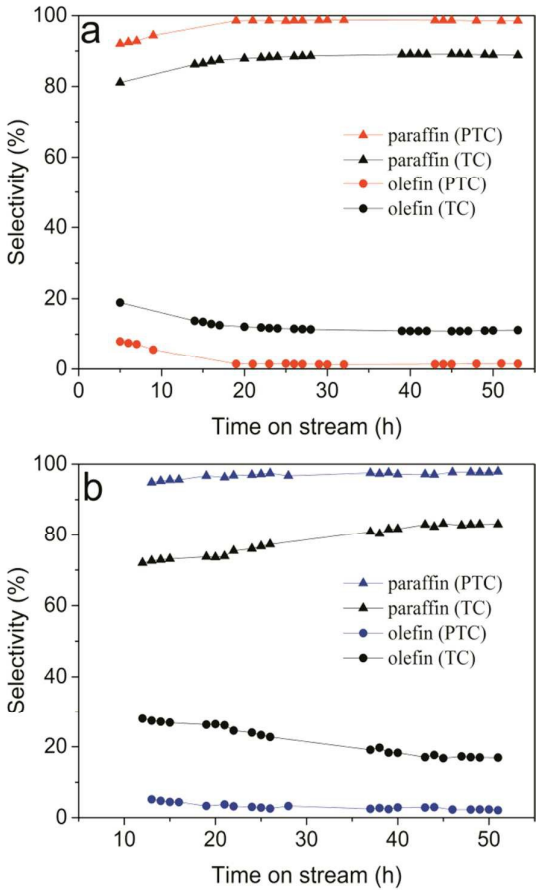

Fig. 10 C_2-C_4 paraffin/olefin distribution under two catalytic conditions for Co/TNT catalysts: (a) 20% Co/TNT; (b) 30% Co/TNT.

metals took part in the hydrogenation reaction as a active component, resulting in partial olefin hydrogenation. Interestingly, UV irradiation significantly increased the formation rate of alkane at 220 °C, and the concentration of alkane produced at 220 °C with the UV irradiation was 1.32 times larger than that produced at 220°C without the UV irradiation. Schumacher et al. have discovered that H_2 molecules can be dissociated into two neutral atoms under intense light irradiation.[65] Combined our experimental results with the relative reports together, when employing UV irradiation, we thought that the conversion from olefin to paraffin was promoted by hydrogen atoms which were dissociatively produced from H_2 molecules, accompanying the activation of C=C bond. Subsequently, the hydrogen atom jumped to the olefin molecule to form corresponding alkanes. A possible reaction mechanism is proposed as follow, schematically. Thus, the hydrogenation reaction of alkene to alkane was promoted by UV illumination even without catalyst. Therefore, the photochemical reaction was one of the important paths for light alkane formation in the gaseous range. Combining the previous analysis, it was evident that UV illumination in FTS would favor hydrogenation of olefin and hydrogenolysis of the long-chain hydrocarbons, leading to the

View Article Online
DOI: 10.1039/C7CY02304A
Journal Name ARTICLE

higher selectivity toward the lighter paraffin products (methane, paraffin in C_2–C_4).

$$H_2 \xrightarrow[220\ ^{o}C]{\text{metal (Ni,Fe)}} 2H$$

$$R_1CH{=}CHR_2 + 2H \longrightarrow R_1CH{=}CHR_2\ (R_1, R_2\text{: H or alkyl})$$

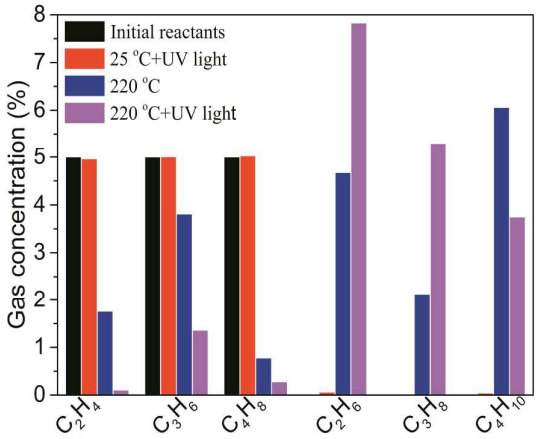

Fig. 11 Concentrations of C_2–C_4 alkenes, alkanes, in the absence of catalyst after 20 h under different conditions. The initial concentrations were 5% C_2H_4, 5% C_3H_6, 5% C_4H_8 and 85% H_2, respectively. Total pressure: 2.0 MPa.

4. Conclusions

In summary, TNT supported cobalt catalyst was successfully applied as a model system to deduce the contribution of UV illumination to the overall Fischer–Tropsch activity and selectivity. From comparison of the performance of photothermocatalytic and solely thermocatalytic FTS, it was concluded that photocatalysis can significantly improve the catalytic performance of FTS. The enhanced CO conversion efficiency could be attributed to the photogenerated electrons transfer from TiO_2 to active Co site, which caused the Co sites with increased surface electron density and subsequently enhanced the adsorption and activation of CO molecules at Co sites. In addition, UV illumination caused an increase of lower molecular weight paraffin and a decrease of CO_2 formation in the FTS product distribution. The increase in light paraffin selectivity was caused by photo-promoted hydrogenation of olefin and hydrogenolysis of the long-chain hydrocarbons, while the decrease of CO_2 selectivity was probably related to the photogenerated holes which restrained WGS reaction. Our approach provided a simple and energy-saving clue to enhance FTS performance and modulate product selectivity. Through optimizing the proper illumination condition (such as wavelength, light intensity), it is possible to gain desirable activity and product distribution in the future.

Table 3 The respective hydrocarbon concentrations under different conditions.

Condition		Concentration (%)					
		C_2H_4	C_2H_6	C_3H_6	C_3H_8	C_4H_8	C_4H_{10}
No illumination	25 °C	5.00	0	5.00	0	5.00	0
	220 °C	1.76	4.68	3.81	2.14	0.80	6.06
UV illumination	25 °C	4.96	0.06	5.00	0.02	5.01	0.04
	220 °C	0.10	7.83	1.36	5.30	0.28	3.75

Acknowledgements

This work was supported by the financial support from the National Natural Science Foundation of China (grant no. 21461017), the specialized research fund for the doctoral program of higher education (grant no. 20131501110001) and Prairie Excellence Innovation and Entrepreneurial Team of Inner Mongolia (grant no. 201201).

Notes and references

1 J. Kang, S. Zhang, Q. Zhang and Y. Wang, Angew. Chem., Int. Ed., 2009, **121**, 2603–2606.
2 I. Puskas and R. S. Hurlbut, Catal. Today, 2003, **84**, 99–109.
3 A. Y. Khodakov, W. Chu and P. Fongarland, Chem. Rev., 2007, **107**, 1692–1744.
4 H. Karaca, O. V. Safonova, S. Chambrey, P. Fongarland, P. Roussel, A. Griboval-Constant, M. Lacroix and A. Y. Khodakov, J. Catal., 2011, **277**, 14–26.
5 G. L. Bezemer, J. H. Bitter, H. P. C. E. Kuipers, H. Oosterbeek, J. E. Holewijn, X. D. Xu, F. Kapteijn, A. J. V. Dillen and K. P. D. Jong, J. Am. Chem. Soc., 2006, **128**, 3956–3964.
6 A. A. Muleja, Y. Yao, D. Glasser and D. Hildebrandt, Appl. Catal., A, 2016, **517**, 217–226.
7 X. B. Chen and S. S. Mao, Chem. Rev., 2007, **38**, 2891–2959.
8 D. Heyl, U. Rodemerck and U. Bentrup, ACS Catal., 2016, **6**, 6275–6284.
9 B. Rungtaweevoranit, J. Baek, J. R. Araujo, B. S. Archanjo, K. M. Choi, O. M. Yaghi and G. A. Somorjai, Nano Lett., 2016, **16**, 7645–7649.
10 B. Ma, Y. Y. Wang, X. L. Tong, X. N. Guo, Z. F. Zheng and X. Y. Guo, Catal. Sci. Technol., 2017, **7**, 2805–2812.
11 M. Q. Yang, B. Weng and Y. J. Xu, J. Mater. Chem. A, 2014, **2**, 1710–1720.
12 P. Sharma and Y. Sasson, Green Chem., 2017, **19**, 844–852.

View Article Online
DOI: 10.1039/C7CY02304A

13 C. H. Hao, X. N. Guo, Y. T. Pan, S. Chen, Z. F. Jiao, H. Yang and X. Y. Guo, J. Am. Chem. Soc., 2016, **138**, 9361–9364.
14 N. X. Li, M. Liu, B. Yang, W. X. Shu, Q. H. Shen, M. C. Liu and J. C. Zhou, J. Phys. Chem. C , 2017, **121**, 2923–2932.
15 J. H. Xiong, Y. H. Liu, C. S. Cao, L. J. Shen, W. M. Wu, S. J. Liang, R. W. Liang and L. Wu, J. Mater. Chem. A, 2015, **3**, 6935–6942.
16 C. C. Yang, J. Vernimmen, V. Meynen, P. Cool and G. Mul, J. Catal., 2011, **284**, 1–8.
17 X. N. Guo, Z. F. Jiao, G. Q. Jin and X. Y. Guo, ACS Catal., 2015, **5**, 3836–3840.
18 Y. F. Zhao, B. Zhao, J. J. Liu, G. B. Chen, R. Gao, S. Y. Yao, M. Z. Li, Q. H. Zhang, L. Gu, J. L. Xie, X. D. Wen, L. Z. Wu, C. H. Tung and D. Ma, Angew. Chem., Int. Ed., 2016, **55**, 4215–4219.
19 S. Y. Yu, T. Zhang, Y. H. Xie, Q. H. Wang, X. C. Gao, R. F. Zhang, Y. L. Zhang and H. Q. Su, Int. J. Hydrogen Energy, 2015, **40**, 870–877.
20 Q. H. Zhang, J. C. Kang and Y. Wang, ChemCatChem, 2010, **2**, 1030–1058.
21 A. Y. Khodakov, A. Griboval-Constant, R. Bechara, and V. L. Zholobenko, J. Catal., 2002, **206**, 230–241.
22 J. A. Delgado, C. Claver, S. Castillón, D. Curulla-Ferré, V. V. Ordomsky and C. Godard, Appl. Catal., A, 2016, **513**, 39–46.
23 X. Yang, W. B. Wang, L. P. Wu, X. J. Li, T. J. Wang and S. J. Liao, Appl. Catal., A, 2016, **526**, 45–52.
24 F. Jiang, M. Zhang, B. Liu, Y. B. Xu and X. H. Liu, Catal. Sci. Technol., 2017, **7**, 1245–1265.
25 D. A. Wang, B. Yu, C. W. Wang, F. Zhou and W. M. Liu, Adv. Mater., 2009, **21**, 1964–1967.
26 J. Wang, L. Zhao, V. S. Y. Lin and Z. Q. Lin, J. Mater. Chem., 2009, **19**, 3682–3687.
27 M. Abdullah, S. K. Kamarudin and L. K. Shyuan, Nanoscale Res. Lett., 2016, **11**, 553.
28 L. Fan, N. Ichikuni, S. Shimazu and T. Uematsu, Appl. Catal., A, 2003, **246**, 87–95.
29 H. Häkkinen and U. Landman, J. Am. Chem. Soc., 2001, **123**, 9704–9705.
30 K. Yang, J. F. Liu, R. R. Si, X. Chen, W. X. Dai and X. Z. Fu, J. Catal., 2014, **317**, 229–239.
31 X. M. Sun and Y D. Li, Chem. Eur. J., 2003, **9**, 2229–2238.
32 F. Morales, F. M. De Groot, O. L. J. Gijzeman, A. Mens, O. Stephan and B. M. Weckhuysen, J. Catal., 2005, **230**, 301–308.
33 X. H. Zhang, H. Q. Su and X. Z. Yang, J. Mol. Catal. A: Chem., 2012, **360**, 16–25.
34 S. Bala, I. Mondal, A. Goswami, U. Pal and R. Mondal, J. Mater. Chem. A, 2015, **3**, 20288–20296.
35 K. Shimura, T. Miyazawa, T. Hanaoka and S. Hirata, Appl. Catal., A, 2015, **494**, 1–11.
36 G. Jacobs, T. K. Das, Y. Q. Zhang, J. L. Li, G. Racoillet and B. H. Davis, Appl. Catal., A, 2002, **233**, 263–281.
37 S. F. Mu, D. B. Li, B. Hou, J. G. Chen and Y. H. Sun, Catal. Lett., 2009, **133**, 341–345.
38 B. M. Reddy, B. Chowdhury, I. Ganesh, E. P. Reddy, T. C. Rojas and A. Fernandez, J. Phys. Chem. B, 1998, **102**, 10176–10182.
39 D. Barreca, A. Devi, R. A. Fischer, D. Bekermann, A. Gasparotto, A. Gavagnin, C. Maccato, E. Tondello, E. Bontempi, L. E. Depero and C. Sada, CrystEngComm, 2011, **13**, 3670–3673
40 L. Y. Wu, Z. Li, D. Z. Han, J. H. Wu and D. K. Zhang, Fuel Process. Technol., 2015, **134**, 449–455.
41 F. L. Wang, Y. J. Jiang, A. Gautam, Y. R. Li and R. Amal, ACS Catal., 2014, **4**, 1451–1457.
42 T. Ohsaka, F. Izumi and Y. J. Fujiki, Raman Spectrosc., 1978, **7**, 321–324.
43 Y. Lei, L. D. Zhang and J. C. Fan, Chem. Phys. Lett., 2001, **338**, 231–236.
44 J. G. Cai, C. Raptis, Y. S. Raptis and E. Anastassakis, Phys. Rev. B, 1995, **51**, 201–209.
45 Y. L. Zheng, W. Z. Wang, D. Jiang and L. Zhang, Chem. Eng. J., 2016, **284**, 21–27.
46 J. Li, G. Z. Lu, G. S. Wu, D. S. Mao, Y. L. Guo, Y. Q. Wang and Y. Guo, Catal. Sci. Technol., 2014, **4**, 1268–1275.
47 S. Y. Yu, Y. Ma, Y. X. Zhi, H. Jing and H. Q. Su. Integr. Ferroelectr., 2013, **147**, 59-66.
48 K. Shimura, T. Miyazawa, T. Hanaoka and H. Satoshi, Appl. Catal., A, 2013, **460-461**, 8-14.
49 Y. Ma, X. L. Wang, Y. S. Jia, X. B. Chen, H. X. Han and C. Li, Chem. Rev., 2014, **114**, 9987–10043.
50 P. D. Tran, L. F. Xi, S. K. Batabyal, L. H. Wong, J. Barber and J. S. C. Loo, Phys. Chem. Chem. Phys., 2012, **14**, 11596–11599.
51 W. Chanmanee, M. F. Islam, B. H. Dennis and F. M. MacDonnell, Proc. Natl. Acad. Sci. U. S. A., 2016, **113**, 2579–2584.
52 M. S. Hamdy, R. Amrollahi, I. Sinev, B. Mei and G. Mul, J. Am. Chem. Soc., 2013, **136**, 594–597.
53 X. H. Lin, K. Yang, R. R. Si, X. Chen, W. X. Dai and X. Z. Fu, Appl. Catal., B, 2014, **147**, 585–591.
54 D. Z. Wang, X. P. Cheng, Z. E. Huang, X. Z. Wang and S. Y. Peng, Appl. Catal., 1991, **77**, 109–122.
55 X. H. Lin, L. L. Lin, K. Huang, X. Chen, W. X. Dai and X. Z. Fu, Appl. Catal., B, 2015, **168**, 416–422.
56 D. C. Song and J. L. Li, J. Mol. Catal. A: Chem., 2006, **247**, 206–212.
57 J. S. Zou, Z. C. Si, Y. D. Cao, R. Ran, X. D. Wu and D. Weng, J. Phys. Chem. C, 2016, **120**, 29116–29125.
58 A. Kudelski and B. Pettinger, Chem. Phys. Lett., 2004, **383**, 76–79.
59 S. C. Chang, A. Hamelin and M. J. Weaver, Surf. Sci., 1990, **239**, L543–L547.
60 Y. Zhang, M. Koike, R. Q. Yang, S. Hinchiranan, T. Vitidsant and N. Tsubaki, Appl. Catal., A, 2005, **292**, 252–258.
61 N. Tsubaki, S. Sun and K. Fujimoto, J. Catal., 2001, **199**, 236–246.
62 A. Tavasoli, K. Sadagiani, F. Khorashe, A. A. Seifkordi, A. A. Rohani and A. Nakhaeipour, Fuel Process. Technol., 2008, **89**, 491–498.
63 M. Anpo, N. Aikawa, and Y. Kubokawa, J. Phys. Chem., 1984, **88**, 3998-4000.
64 M. Anpo, M.Takeuchi, J. Catal., 2003, **216**, 505-516.
65 A. Zavriyev, P. H. Bucksbaum, H. G. Muller and D. W. Schumacher, *Phys. Rev. A,* 1990, **42**, 5500-5514.

View Article Online
DOI: 10.1039/C7CY02304A

Table of contents